



## Experimental and theoretical investigation of heat and mass transfer processes during wood pyrolysis

Won Chan Park<sup>a</sup>, Arvind Atreya<sup>a,\*</sup>, Howard R. Baum<sup>b</sup>

<sup>a</sup> Department of Mechanical Engineering, University of Michigan, 2158 GGBL 2350 Hayward St., Ann Arbor, MI 48109, USA

<sup>b</sup> Department of Fire Protection Engineering, University of Maryland, 3106-D J.M. Patterson Building, College Park, MD 20742, USA

### ARTICLE INFO

#### Article history:

Received 24 May 2009

Received in revised form 7 August 2009

Accepted 14 October 2009

Available online 26 November 2009

#### Keywords:

Biomass

Wood

Charring materials

Pyrolysis

Thermal decomposition

### ABSTRACT

Thermal decomposition of 25.4 mm diameter dry wood spheres is studied both experimentally and theoretically. Wood spheres were pyrolyzed in a vertical tube furnace at temperatures ranging from 638 K to 879 K. Mass loss and temperatures of the sample were measured during pyrolysis. Center temperature measurements showed two distinct thermal events consisting of sequential endothermic and exothermic reactions. A numerical investigation of these endo/exothermic reactions using various pyrolysis kinetics models was conducted to determine the pyrolysis mechanism and the heats of the pyrolysis reactions. A comparison of the experimental and numerical results showed that (i) Contrary to the suggestions in the literature, the contributions of the secondary tar decomposition and lignin decomposition to the center temperature exothermic peak are small. (ii) Exothermic decomposition of the intermediate solid is responsible for the center temperature peak. (iii) The center temperature plateau is caused by the endothermic decomposition of cellulose. (iv) Internal pressure generation was found to be quite important because it controls the pyrolyzate mass transfer and thus affects both the heat transfer and the residence time of the pyrolysis gases for secondary decomposition.

Based on the experimental and numerical results, a new wood pyrolysis model is proposed. The model consists of three endothermic parallel reactions producing tar, gas and intermediate solid and subsequent exothermic decomposition of the intermediate solid to char and exothermic decomposition of tar to char and gas. The proposed pyrolysis model shows good agreement with the experiments.

Pressure calculations based on the new pyrolysis model revealed that high pressure is generated inside the biomass particle during pyrolysis and sample splitting was observed during the experiments. The splitting is due to both weakening of the structure and internal pressure generation during pyrolysis. At low heating rates, structural weakness is the primary factor, whereas at high heating rates, internal pressure is the determining factor. It is expected that moisture, while not considered in this work will have a similar effect, but at lower temperatures.

© 2009 The Combustion Institute. Published by Elsevier Inc. All rights reserved.

### 1. Introduction

Biomass is expected to be a major source of sustainable energy in the future as the World transitions from traditional carbon-based fuels such as coal, petroleum and natural gas to carbon-neutral fuels to combat global warming and fossil fuel depletion. As recognized in Ref. [1], biomass-derived bio-fuels are the only current sustainable source of liquid hydrocarbons required for transportation. However, an economic way of making them has not yet been devised despite the fact that lignocellulosic biomass costs significantly less than crude oil (about \$15 per barrel of oil energy equivalent). The US forests, crops, and urban wood wastes can produce 1.3 billion dry tons of renewable biomass per year, without

land use change [2]. Land use change is an important consideration because using good cropland for the production of bio-fuels exacerbates the very global warming problem they attempt to solve [3]. Further, if the excess forest biomass is not harvested, it only serves to produce devastating forest fires. If harvested, it can provide a significant amount of carbon-neutral liquid bio-fuels for transportation use. Harvesting the excess forest biomass also makes the forest healthy. Forestry data shows that well-managed healthy forests grow 55% faster. Thus, extraction of this forest biomass is better than carbon neutral.

Barriers to usage of this biomass are (i) It is voluminous – resulting in low energy density. (ii) It is distributed over large and remote areas. (iii) The cost of transportation from remote locations to a central processing facility is high. (iv) It is chemically diverse making biochemical fermentation techniques difficult, and (v) The method of waste disposal (minerals, ash, etc.) that is generated during

\* Corresponding author. Fax: +1 734 647 3170.

E-mail address: [aatreya@umich.edu](mailto:aatreya@umich.edu) (A. Atreya).

## Nomenclature

$A$	pre-exponential constant ( $s^{-1}$ )
$B$	permeability ( $m^2$ )
$C$	specific heat capacity ( $J/kg\ K$ )
$C_p$	constant pressure specific heat capacity ( $J/kg\ K$ )
$d$	pore size (m)
$e$	emissivity
$E$	activation energy ( $J/mol\ K$ )
$f$	initial cellulose mass fraction
$F$	view factor
$h$	heat transfer coefficient ( $W/m^2\ K$ )
$k$	reaction rate ( $s^{-1}$ )
$M$	molecular weight (kg/mol)
$P$	pressure
$P_0$	ambient pressure (101,300 Pa)
$P_c$	pressure at center (Pa)
$P_m$	pressure at $r = \frac{r_0}{2}$ (Pa)
$P_t$	tar partial pressure (Pa)
$P_g$	gas partial pressure (Pa)
$Q$	heat generation ( $W/m^3$ )
$r$	radius (m)
$r_0$	radius of wood sphere (m)
$R$	universal gas constant (8.314 J/mol K)
$S$	mass generation ( $kg/m^3\ s$ )
$t$	time (s)
$T$	temperature (K)
$T_{fn}$	furnace temperature (K)
$T_p$	pyrolysis temperature (K)
$V$	flow velocity (m/s)
$Y$	solid mass fraction

## Greek letters

$\gamma$	char yield fraction
$\varepsilon$	porosity
$\eta$	degree or extent of pyrolysis
$\Delta h$	heat of pyrolysis ( $J/kg$ )
$\lambda$	thermal conductivity ( $W/m\ K$ )
$\mu$	viscosity ( $kg/m\ s$ )
$\rho$	density ( $kg/m^3$ )
$\sigma$	Stefan–Boltzmann constant ( $5.67 \times 10^{-8}\ W/m^2\ K$ )
$\omega$	cellulose mass fraction

## Superscript

$m, n$	power constants for cellulose decomposition reaction
--------	--

## Subscripts

$A, B$	cellulose fractions
$a$	virgin solid
$c$	char, primary char generation reaction
$c2$	secondary char generation reaction
$cl$	cellulose
$fn$	furnace
$g$	gas, primary gas generation reaction
$g2$	secondary gas generation reaction
$hcl$	hemicellulose
$is$	intermediate solid
$l$	lignin
$s$	surface
$t$	tar
$v$	total volatiles
$w$	initial virgin solid
$0$	initial condition

processing at a central facility is important for sustainable forests and crops. The recent Tennessee toxic coal ash sludge spill points to the importance of proper disposal of the waste generated at any central processing facility. While it may be toxic to humans, it contains essential nutrients for sustainable plant growth.

Currently available pyrolysis methods for conversion of this biomass to liquid transportation fuels require small particle size ( $\sim 1$  mm) and several times the amount of catalyst [4]. This is clearly not possible with the widely distributed 1.3 billion dry tons of renewable biomass supply available per year [2]. Thus, an economical way has to be found to process this biomass on-site without finely grinding it. The present work is a step toward this goal. Here we attempt to understand and model the behavior of wood chipper-size ( $\sim 1$  in.) particles during pyrolysis.

Wood pyrolysis is a complex process. It involves many physical and chemical processes such as heat transfer, moisture evaporation, decomposition kinetics, heat of pyrolysis, pressure build up in the solid, changes in material properties with the extent of pyrolysis and temperature, anisotropic property behavior, among others. To add to these complications, our experimental measurements show that during the pyrolysis of moisture-free wood spheres, a distinct center temperature plateau appears between 610 and 640 K owing to an endothermic reaction. Further, immediately after the endothermic reaction, the center temperature rises sharply and exceeds the surface temperature due to an exothermic reaction. Thus, from a thermal perspective, wood pyrolysis is a combination of successive endothermic and exothermic reactions. Similar observations have been reported by other researchers in the literature [5–9] but the current wood pyrolysis models do not account for this phenomenon. Nevertheless, it is important for determining the energy required to convert solid wood to liquid bio-fuels and from the point-of-view of

internal pressure generation that may split the particle. A single heat of pyrolysis, ' $\Delta h$ ' of lignocellulosic materials is quoted in the literature. It varies greatly depending on the type of material, experimental setup and conditions. Values found in the literature range from 0 to  $\pm 1500$  kJ/kg [7,10].

Bilbao et al. [5] measured  $\Delta h$  of Pinus Pinaster using DSC (differential scanning calorimeter) in order to use it as input data for their wet wood pyrolysis model. They expressed their results as: for the first endothermic reaction stage (up to 60% conversion)  $\Delta h = 274$  kJ/kg and for the second exothermic reaction stage (remaining 40% conversion)  $\Delta h = -353$  kJ/kg. They presumed that the first endothermic reaction corresponds to cellulose and hemicellulose decomposition and lignin decomposition accounts for the second exothermic reaction. Di Blasi et al. [6] reported that the inner core of the wood cylinder decomposition showed endo/exothermic reactions. They observed that the two reactions are more distinguishable at lower heating rates. At higher heating rates, the endothermic and exothermic reactions overlap producing a smaller temperature peak at the center. They also explained this thermal behavior by presuming endothermic decompositions of holocellulose and extractives and exothermic lignin decomposition. Koufopoulos et al. [7] also measured the center temperature of dry wood cylinders during pyrolysis and obtained results similar to Di Blasi et al's [6]. However, they attributed the center temperature peak to the exothermic secondary reaction between volatiles and char. Strezov et al. [9] measured the heat of pyrolysis ' $\Delta h$ ' of cellulose, hemicellulose, lignin and four different sawdust biomass samples in an infrared furnace. They reported that all of the samples showed both endothermic and exothermic reactions during pyrolysis. They attributed the exothermic behavior to the exothermic tar cracking [11] and the decomposition of dehydrocellulose [8,12].

From this previous work, a few facts are clear (i) Both endothermic and exothermic reactions have been observed previously by several investigators in addition to this work. However, the explanations for this behavior differ significantly. The reaction mechanism has not been clarified. (ii) The rates of the reactions involved and the heats of these reactions also have not been quantified.

For thick wood particles, internal pressure generation is also an important factor influencing the pyrolysis process and the temperature. Pressure gradient drives the volatiles out of the particle and high internal pressure may also split a partially pyrolyzed wood particle. Pressure splitting of thick particles may be desirable because it obviates the need to make small particles. This natural formation of small particles enhances the biomass conversion speed and increases the yield of liquid products. It also reduces the residence time of the volatiles in the pores reducing tar cracking that would otherwise be promoted by high pressure.

There is a substantial amount of literature on thermal decomposition of lignocellulosic materials, however, only a few studies have considered pressure generation during pyrolysis. This is partly due to the nonlinear equations describing pressure generation. Fredlund [13] measured pressure variations at multiple locations in a pyrolyzing thick block of wood. Baum and Atreya [14] analytically solved the pressure distribution in a pyrolyzing charring solid undergoing flame spread. Park et al. [15] developed a numerical model to solve for pressure generation during wood pyrolysis. Internal pressure measurements and/or models have not been reported for pyrolysis of chipper-size wood particles. The small sample size makes the pressure measurement very difficult and it is usually assumed that the gases that are generated simply leave the particle. In this work, internal pressure generation in chipper-size spherical wood particles is numerically investigated. The objective is to provide a better understanding of wood pyrolysis with emphasis on quantifying the heat and mass transfer that occurs during pyrolysis. We employ both experimental and numerical methods to develop a wood pyrolysis model useful for producing liquid bio-fuels from chipper-size ( $\sim 1$  in.) biomass particles.

## 2. Experiment setup

Pyrolysis experiments were conducted on moisture free maple wood spheres 1" in diameter. Spherical geometry was used to maintain one dimensionality for ease of modeling. Weight and temperature changes of the sample during pyrolysis were measured. The apparatus used is schematically shown in Fig. 1a. These spheres were heated in the vertical tube furnace at temperatures ranging from 638 to 879 K. The tube furnace (Carbolite® GVA 12/300) consists of a mullite tube (length: 558 mm, inner diameter: 106 mm), two electric heaters (total heating length: 300 mm), a temperature controller, insulators and a stainless steel outer casing.

As shown in Fig. 1a, weight loss of the sample was measured by a scale located above the furnace. Sample surface temperature was measured by a *K*-type thermocouple (bead diameter  $\sim 0.2$  mm). The thermocouple bead was positioned in a tiny slit on the surface of the sample and fixed by glue. Temperatures inside the sample were measured at two locations, center ( $r = 0$ ) and middle ( $r = r_0/2$ ) by two thin sheathed *K*-type thermocouple probes (0.25 mm sheath diameter, 450 mm length) inserted through holes drilled in the sample. The probe holes were always drilled in the radial direction because it was easy to identify. Fig. 1b shows the installation of thermocouples in the sample. Furnace temperatures were monitored by eight thermocouples on the tube inside surface and two thermocouples on the top and bottom end insulating caps. From temperature measurements at 10 locations on the furnace, the

effective furnace temperature  $T_{fn}$  was calculated by the following equation.

$$T_{fn} = \left( \sum_i F_i T_i^4 \right)^{0.25}, \quad i = 1 \dots 10 \quad (1)$$

where,  $F_i$  is the view factor between the *i*th section area of the furnace inside surface and the sample surface [16].

Argon at ambient temperature was used to purge the furnace at a low flow rate of 0.21 g/s to displace oxygen and carry away the pyrolysis products. Gas temperature near the sample was also measured by a *K*-type thermocouple to determine the convective heat losses. The voltage signals from all the thermocouples were processed by two NI-SCXI-1112 (8 channels) boards installed in a PXI-1011 chassis. The temperature data was recorded at 1 Hz frequency.

The wood spheres were dried at a temperature of 115 °C for at least 3 h before the pyrolysis experiments to remove moisture. In order to avoid interference in the mass loss measurement due to the installation of temperature probes in the sample, mass measurements and temperature measurements were conducted separately for the same conditions.

## 3. Experimental results

Wood sphere pyrolysis experiments were conducted at six different furnace temperatures ranging from 638 K to 879 K. Fig. 2 shows the measured solid mass fraction ( $Y = \text{sample weight}/\text{initial sample weight}$ ). As the furnace temperature increases from 638 K to 879 K, the final char yield decreases from 31% to 17% of the initial sample mass, whereas mass loss rate increases. Wood sphere pyrolysis begins with low temperature hemicellulose decomposition showing a mild weight loss rate. As the temperature increases, cellulose and lignin start to decompose and the solid mass fraction decreases rapidly. The majority of weight loss occurs during this period. After the completion of cellulose decomposition, the leftover lignin continues to decompose resulting in a gradual weight loss rate.

Temperature measurements at the surface and at the center of the sample are shown in Fig. 3. The surface temperature rises quickly and attains thermal equilibrium with the furnace. Center temperature measurements show distinct plateaus in the temperature range of 610–640 K, indicating an endothermic reaction. Immediately after completion of the endothermic reaction, the center temperatures rise sharply owing to the subsequent exothermic reaction. During the exothermic reaction, the center temperatures exceed the surface temperature by 10–70 K except for 879 K case where it still rises sharply but the surface temperature also rises sharply. While the center temperature peaks are more distinct for the low temperature cases (688–783 K), exothermicity exists for all cases as shown in Fig. 14. For high furnace temperatures, the center temperature peaks are not as obvious because of the overlap between the endo- and exo-thermic reactions. The exothermicity of the second reaction enables heating of the entire sample to occur with only a short time lag after the surface. It is evident in Fig. 3 for the high temperature experiments. This is an important observation because large internal pressure is generated under high temperature conditions that may split the sample. An example of this split is shown in Fig. 1b. Thus, the sample size is naturally reduced for producing liquid hydrocarbons via fast pyrolysis.

An interesting comparison of solid mass loss and temperature for  $T_{fn} = 688$  K is shown in Fig. 4. It indicates that the temperature plateau corresponds to the second half of the active mass loss period and gradual or negligible mass loss occurs during the center temperature peak. This was true for all the experiments conducted at different furnace temperatures.

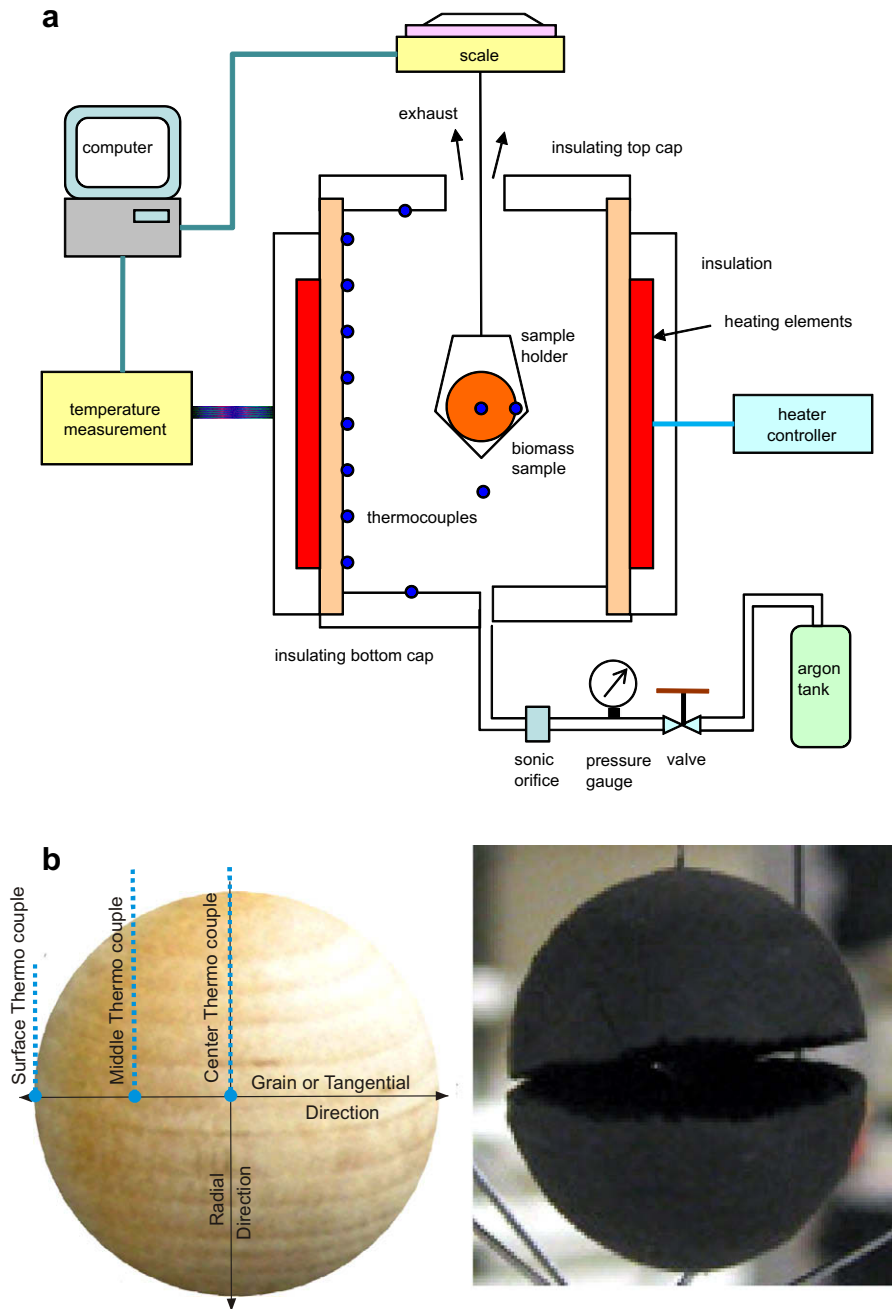


**Fig. 1.** (a) Schematic of the experimental apparatus. (b) Photographs of the sample before and after the experiment. The sample before the experiment shows the location of the installed thermocouples. The thermocouples probe holes were drilled in the radial direction because it was the easiest to identify. A pressure-split sample held in the sample holder after the experiment is also shown.

It is generally accepted that endothermicity during biomass pyrolysis is caused by the formation of tar or volatiles. Meanwhile, several mechanisms have been proposed to explain the exothermic behavior. These are, exothermic lignin decomposition, secondary tar cracking reactions, and dehydrocellulose decomposition to gas and char. These exothermic reaction mechanisms are evaluated in the next section with the help of the experimental results.

#### 4. Thermal mechanism of wood pyrolysis

Various endo/exothermic mechanisms available in the literature were investigated numerically to determine their effect on thermal characteristics of wood pyrolysis and to determine the reason for the center temperature peak.

#### 4.1. Model descriptions

Three different models were used with the experimental measurements. In this section, characteristics and kinetics of the models are described. The kinetic schemes and the governing equations for the models are listed in Tables 1 and 2.

##### 4.1.1. Model-1 [17]

In this model, wood is assumed to decompose into three major products: tar, char and gas, by three primary reactions. And then, a portion of tar decomposes to gas and char by successive secondary reactions [17]. The kinetic parameters and heats of pyrolysis of the secondary reactions for model-1 were obtained from the literature and they are listed in Table 3. To determine if the model will ex-

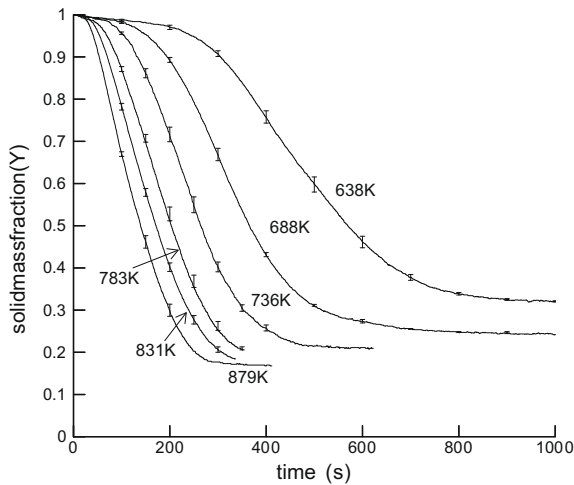


Fig. 2. Solid mass fraction measurements for different average furnace temperatures.

plain the experimental results, the heats of pyrolysis for primary reactions were obtained by fitting with the experimental measurements [30].

#### 4.1.2. Model-2 [18–22]

Wood consists of three major components: hemicellulose (25–35%), cellulose (40–50%) and lignin (16–33%). Each component shows different characteristics during its thermal decomposition. Hemicellulose decomposition occurs at 200–260 °C and produces acetic acid. Cellulose decomposes to levoglucosan and dehydrocellulose at 240–350 °C. Lignin decomposes over a broad temperature range of 280–500 °C and produces more char than the other two components [18]. Model-2 regards wood as the mixture of these three major components. This model is useful to analyze the effect of decomposition of individual wood components. In model-2, the kinetic parameters of each component were chosen from the literature values that showed good agreement with the author's experiments. The following parameters were chosen: hemicellulose [19]; cellulose [20]; lignin [21]. Unlike model-1, wood in model-2 decomposes to two final products; char and volatiles. This was necessary because a three-product model is not available for hemicellulose and lignin. Thus, volatiles account for the sum of gas and

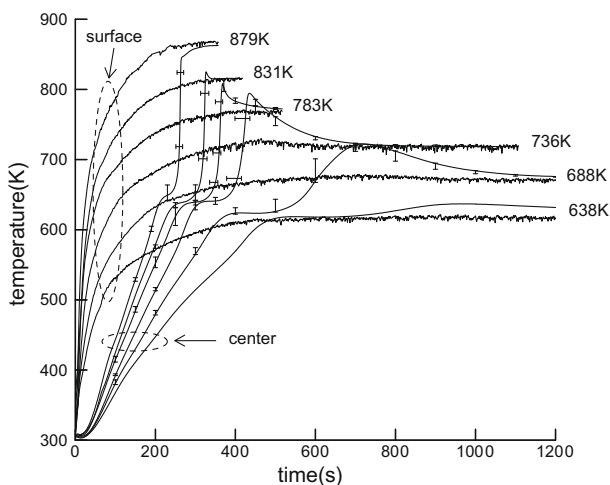


Fig. 3. Temperature measurements at the center ( $r=0$ ) and at the surface of the sample.

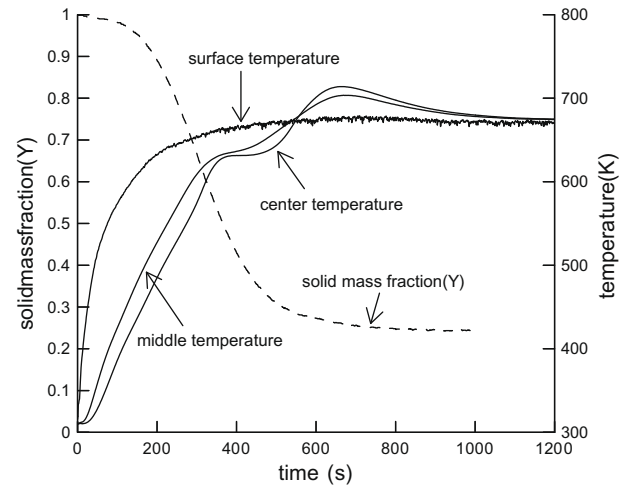


Fig. 4. Solid mass fraction and temperatures of wood sphere pyrolysis at 688 K.

tar. Also, the char yield  $\gamma$  for model-2 is pre-determined. The mass fractions for hemicelluloses, cellulose, and lignin are: 30%, 43.6%, and 26.4% respectively [22]. The extractives portion is included in hemicelluloses. The individual models are:

**4.1.2.1. Hemicellulose.** Hemicellulose decomposition is modeled by a two-step reaction [19]. First, hemicellulose decomposes to volatiles and intermediate solid, and then the intermediate solid decomposes to volatiles and char in the subsequent reaction. The kinetic parameters of hemicellulose pyrolysis are listed in Table 4.

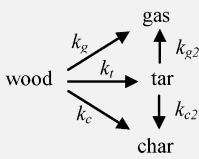
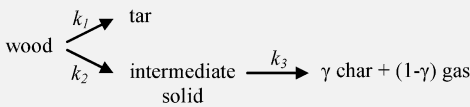
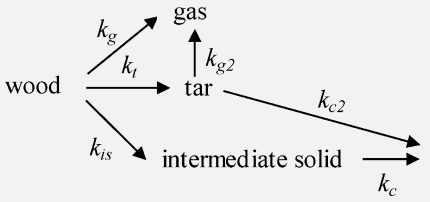
**4.1.2.2. Cellulose.** Cellulose pyrolysis is modeled by two parallel reactions [20]. Initial mass fractions of cellulose for the two components are pre-determined as:  $\rho_{clA,0} = f_A \rho_{cl,0}$ ,  $\rho_{clB,0} = f_B \rho_{cl,0}$ .  $\Delta h$ 's of the two reactions are assumed to be the same. The kinetic parameters of cellulose pyrolysis are listed in Table 5.

**4.1.2.3. Lignin.** Lignin decomposes to volatiles and char by a single Arrhenius type reaction [21]. The kinetic parameters of lignin pyrolysis are listed in Table 6.

#### 4.1.3. Model-3 [23,24]

Model-3 has the structure of the Kilzer–Broido cellulose pyrolysis model [23]. Originally, the Kilzer–Broido model was postulated for three reactions of cellulose decomposition; the slightly endothermic reaction from cellulose to dehydrocellulose, the strong endothermic tar (mainly levoglucosan) formation from cellulose and the exothermic decomposition of dehydrocellulose to char and gas. Milosavljevic and colleagues reported that the enthalpy of cellulose pyrolysis becomes more endothermic as char yield decreases, based on their experiment and the literature [8,24]. Their experimental results support the exothermic char formation mechanism of the Kilzer–Broido model. Wood pyrolysis experiments in this work showed thermal behavior similar to the cellulose pyrolysis experiment by Milosavljevic et al. One reason may be that approximately half of the wood by mass consists of cellulose. Hence, it is plausible to apply the Kilzer–Broido type model to wood pyrolysis. In model-3, wood is pyrolyzed through two paths. One is an endothermic tar producing reaction and the other is an intermediate solid producing reaction which is assumed to have a zero heat of pyrolysis. The intermediate solid, corresponding to dehydrocellulose in the Kilzer–Broido model, is decomposed into char and gas by an exothermic reaction. Each reaction rate is assumed to follow a 1st order Arrhenius reaction. The activation energy of reaction 1 is taken from the wood to tar producing reaction

**Table 1**  
Kinetics of model-1, -2, -3 and the proposed model.

<i>kinetics</i>	
<i>Model-1</i>	 $k_i = A_i e^{-\frac{E_i}{RT}} \quad i = t, g, c, g2, c2$
<i>Model-2</i>	$\text{hemicellulose} \xrightarrow{k_1} (1-\gamma_1) \text{ volatiles} + \gamma_1 \text{ intermediate solid} \xrightarrow{k_2} (1-\gamma_2) \text{ volatiles} + \gamma_2 \text{ char}$ $k_i = A_i e^{-\frac{E_i}{RT}} \quad i = 1, 2$ <hr/> $\text{cellulose}_A \xrightarrow{A} (1-\gamma_A) \text{ volatiles} + \gamma_A \text{ char}$ $\text{cellulose}_B \xrightarrow{B} (1-\gamma_B) \text{ volatiles} + \gamma_B \text{ char}$ $\frac{d\omega_i}{dt} = -A_i e^{-\frac{E_i}{RT}} \omega_i^n (1-0.99\omega_i)^m \quad i = A, B, \quad \omega_A = \frac{\rho_{clA}}{\rho_{clA,0}}, \quad \omega_B = \frac{\rho_{clB}}{\rho_{clB,0}}, \quad \rho_{cl} = \rho_{clA} + \rho_{clB}$ <hr/> $\text{lignin} \xrightarrow{k_l} (1-\gamma_l) \text{ volatiles} + \gamma_l \text{ char} \quad k_i = A_i e^{-\frac{E_i}{RT}}$
<i>Model-3</i>	 $k_i = A_i e^{-\frac{E_i}{RT}} \quad i = 1, 2, 3$
<i>Proposed model</i>	 $k = A e^{-\frac{E}{RT}}; \text{ given in text}$

of model-1. Other kinetic parameters are found by fitting with the experimental measurements. A fixed Char yield for reaction 3 was assumed as recommended [8]:  $\gamma = 0.65$ .

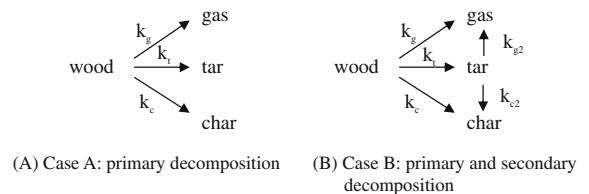
**4.2. Results of Comparison with experiments**

To develop a quantitative understanding of biomass pyrolysis, it is of interest to see how well the above models can reproduce the observed behavior. In particular, an explanation for the exothermic behavior observed during the experiments is sought.

**4.2.1. Secondary tar decomposition**

As shown in the schematic below, the exothermic effect of the secondary tar decomposition was investigated by a comparison between Case A – without secondary tar decomposition and Case B –

with secondary tar decomposition. This comparison was made based on model-1. The kinetics parameters and heats of pyrolysis are listed in Table 3.



Temperatures at the center, middle and surface for Cases A and B are compared in Fig. 5. The temperature difference between Case A and Case B is hardly noticeable, implying that the exothermicity of the secondary tar decomposition is not significant to cause the

**Table 2**  
Governing equations of model-1,-2,-3.

	Model-1	Model-2	Model-3
Solid masses	$\frac{\partial \rho_a}{\partial t} = S_a = -(k_t + k_g + k_c)\rho_a$ $\frac{\partial \rho_c}{\partial t} = S_c = k_c \rho_a + k_{c2} \rho_t$	$\frac{\partial \rho_{hcl}}{\partial t} = S_{hcl} = -k_1 \rho_{hcl}$ $\frac{\partial \rho_{is}}{\partial t} = S_{is} = \gamma_1 k_1 \rho_{hcl} - k_2 \rho_{is}$ $\frac{\partial \rho_{clA}}{\partial t} = S_{clA} = \rho_{clA,0} \frac{d\theta_A}{dt}$ $\frac{\partial \rho_{clB}}{\partial t} = S_{clB} = \rho_{clB,0} \frac{d\theta_B}{dt}$ $\rho_{cl} = \rho_{clA} + \rho_{clB}$ $\frac{\partial \rho_l}{\partial t} = S_l = -k_l \rho_l$ $\frac{\partial \rho_c}{\partial t} = S_c = \gamma_2 k_2 \rho_{is} + \gamma_A S_{clA} + \gamma_B S_{clB} + \gamma_l S_l$	$\frac{\partial \rho_a}{\partial t} = S_a = -(k_1 + k_2)\rho_a$ $\frac{\partial \rho_a}{\partial t} = S_{is} = k_2 \rho_a - k_3 \rho_{is}$ $\frac{\partial \rho_c}{\partial t} = S_c = \gamma k_3 \rho_{is}$
Gas phase masses	$\frac{\partial(\epsilon \rho_v)}{\partial t} + \frac{1}{r^2} \frac{\partial}{\partial r} (r^2 V \rho_t) = S_t = k_t \rho_a - (k_{c2} + k_{g2})\rho_t$ $\frac{\partial(\epsilon \rho_g)}{\partial t} + \frac{1}{r^2} \frac{\partial}{\partial r} (r^2 V \rho_g) = S_g = k_g \rho_a + k_{g2} \rho_t$	$\frac{\partial(\epsilon \rho_v)}{\partial t} + \frac{1}{r^2} \frac{\partial}{\partial r} (r^2 V \rho_v) = S_v = (1 - \gamma_1) k_1 \rho_{hcl}$ $+ (1 - \gamma_2) k_2 \rho_{is} + (1 - \gamma_A) k_A \rho_{clA}$ $+ (1 - \gamma_B) k_B \rho_{clB} + (1 - \gamma_l) k_l \rho_l$ $\frac{\partial(\epsilon \rho_g)}{\partial t} + \frac{1}{r^2} \frac{\partial}{\partial r} (r^2 V \rho_g) = S_g = (1 - \gamma) k_3 \rho_{is}$	$\frac{\partial(\epsilon \rho_v)}{\partial t} + \frac{1}{r^2} \frac{\partial}{\partial r} (r^2 V \rho_t) = S_t = k_1 \rho_a$ $\frac{\partial(\epsilon \rho_g)}{\partial t} + \frac{1}{r^2} \frac{\partial}{\partial r} (r^2 V \rho_g) = S_g = (1 - \gamma) k_3 \rho_{is}$
Total pressure	$\frac{\partial}{\partial t} \left( \frac{\rho P}{T} \right) - \frac{1}{r^2} \frac{\partial}{\partial r} \left( r^2 \frac{BP}{\mu T} \frac{\partial P}{\partial r} \right) = \left( \frac{R}{M_t} S_t + \frac{R}{M_g} S_g \right)$	$\frac{\partial}{\partial t} \left( \frac{\rho P}{T} \right) - \frac{1}{r^2} \frac{\partial}{\partial r} \left( r^2 \frac{BP}{\mu T} \frac{\partial P}{\partial r} \right) + \frac{R}{M_v} S_v$	$\frac{\partial}{\partial t} \left( \frac{\rho P}{T} \right) - \frac{1}{r^2} \frac{\partial}{\partial r} \left( r^2 \frac{BP}{\mu T} \frac{\partial P}{\partial r} \right) = \left( \frac{R}{M_t} S_t + \frac{R}{M_g} S_g \right)$
Energy	$(C_w \rho_a + C_c \rho_c + \epsilon C_{pg} \rho_g + \epsilon C_{pt} \rho_t) \frac{\partial T}{\partial t}$ $+ (C_{pv} \rho_v + C_{pl} \rho_l) V \frac{\partial T}{\partial r} = \frac{1}{r^2} \frac{\partial}{\partial r} \left( r^2 \lambda \frac{\partial T}{\partial r} \right) + Q$	$[C_w (\rho_{hcl} + \rho_{is} + \rho_{cl} + \rho_l) + C_c \rho_c + \epsilon C_{pv} \rho_v] \frac{\partial T}{\partial t}$ $+ C_{pv} \rho_v V \frac{\partial T}{\partial r} = \frac{1}{r^2} \frac{\partial}{\partial r} \left( r^2 \lambda \frac{\partial T}{\partial r} \right) + Q$	$(C_w \rho_a + C_w \rho_{is} + C_c \rho_c + \epsilon C_{pg} \rho_g + \epsilon C_{pt} \rho_t) \frac{\partial T}{\partial t}$ $+ (C_{pv} \rho_v + C_{pl} \rho_l) V \frac{\partial T}{\partial r} = \frac{1}{r^2} \frac{\partial}{\partial r} \left( r^2 \lambda \frac{\partial T}{\partial r} \right) + Q$
Heat generation	$Q = -(k_1 \Delta h_t + k_g \Delta h_g + k_c \Delta h_c) \rho_a$ $- (k_{g2} \Delta h_{g2} + k_{c2} \Delta h_{c2}) \rho_t$	$Q = (S_{hcl} + S_{is}) \Delta h_{hcl} + (S_{clA} + S_{clB}) \Delta h_{cl} + S_l \Delta h_l$	$Q = -(k_1 \Delta h_1 + k_2 \Delta h_2) \rho_a - k_3 \rho_{is} \Delta h_3$

**Table 3**  
Model-1 kinetics parameters and heats of pyrolysis.

Reaction	c	t	g	c2	g2
$A_i$ ( $s^{-1}$ )	$3.27 \times 10^{5a}$	$1.08 \times 10^{10a}$	$4.38 \times 10^{9a}$	$1.00 \times 10^{5b}$	$4.28 \times 10^{6c}$
$E_i$ (J/mol)	111,700 <sup>a</sup>	148,000 <sup>a</sup>	152,700 <sup>a</sup>	108,000 <sup>b</sup>	108,000 <sup>c</sup>
$\Delta h_i$ (kJ/kg)	64 <sup>d</sup>	64 <sup>d</sup>	64 <sup>d</sup>	-42 <sup>e</sup>	-42 <sup>e</sup>

- <sup>a</sup> Ref. [27].
- <sup>b</sup> Ref. [28].
- <sup>c</sup> Ref. [29].
- <sup>d</sup> Ref. [30].
- <sup>e</sup> Ref. [31].

center temperature peak to exceed the surface temperature as observed in the experiments. Therefore, the center temperature peak

in the experiment is not caused by secondary tar decomposition exothermic reactions.

**Table 4**  
Model-2 hemicellulose pyrolysis model parameters [19].

Reaction	1	2
$A_i$	$7.94 \times 10^{16}$	$1.26 \times 10^7$
$E_i$ (J/mol)	195,000	96,000
$\gamma_i$	0.56	0.45

**Table 5**  
Model-2 cellulose pyrolysis model parameters [20].

Reaction	A	B
$A_i$ ( $s^{-1}$ )	$7.94 \times 10^{16}$	$1.26 \times 10^7$
$E_i$ (J/mol)	202,650	255,000
$f_i$	0.821	0.179
$\gamma_i$	0.087	0.087
$n_i$	1	22
$m_i$	0.481	1

**Table 6**  
Model-2 lignin pyrolysis model parameters [21].

Reaction	l
$A_l$ ( $s^{-1}$ )	$5.09 \times 10^5$
$E_l$ (J/mol)	95,000
$\gamma_l$	0.335

**Table 7**  
Material properties and kinetics parameters.

Property	Value	Source
$\rho_w$	630 (kg/m <sup>3</sup> )	Measured
$C_w$	$1500 + 1.0T$ (J/kg K)	[11]
$C_c$	$420 + 2.09T + 6.85 \times 10^{-4} T_2$ (J/kg K)	[11]
$C_{pt}$	$-100 + 4.4T - 1.57 \times 10^{-3} T_2$ (J/kg K)	[11]
$C_{pg}$	$770 + 0.629T - 1.91 \times 10^{-4} T_2$ (J/kg K)	[11]
$C_{pv}$	$0.85C_{pt} + 0.15C_{pg}$	Estimated
$d$	$5 \times 10^{-5} (1 - \eta) + 1 \times 10^{-4} \eta$ (m)	[11]
$e$	1	[31]
$\sigma$	$5.67 \times 10^{-8}$ (W/m <sup>2</sup> K <sup>4</sup> )	
$\lambda_{w,radial}$	0.1046 (W/m K)	[32]
$\lambda_{w,grain}$	0.255 (W/m K)	[32]
$\lambda_{w,tangential}$	0.255 (W/m K)	Estimated
$\lambda_{w,radial}$	0.071 (W/m K)	[32]
$\lambda_{w,grain}$	0.105 (W/m K)	[32]
$\lambda_{w,tangential}$	0.105 (W/m K)	Estimated
$\lambda_v$	0.0258 (W/m K)	[28]
$B_w$	$5 \times 10^{-16}$ (m <sup>2</sup> )	[33]
$B_c$	$1 \times 10^{-13}$ (m <sup>2</sup> )	[33]
$e_w$	0.7	[11]
$e_c$	0.92	[11]
$h$	20 (W/m <sup>2</sup> K)	Estimated
$\mu$	$3.0 \times 10^{-5}$ (kg/m s)	[34]
$M_g$	0.038 (kg/mol)	[11]
$M_t$	0.11 (kg/mol)	[11]
$M_v$	0.076 (kg/mol)	[13]
$R$	8.314 (J/mol K)	

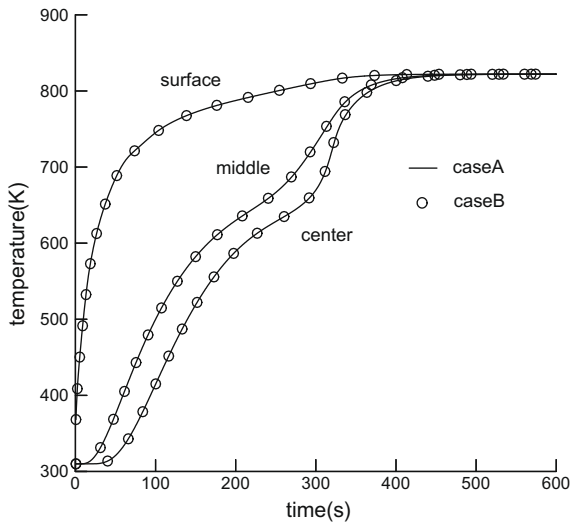


Fig. 5. Temperature comparison between Case A and Case B of model-1 at center, middle and surface; furnace temperature: 831 K.

#### 4.2.2. Lignin decomposition

In the literature [5,6], the exothermic lignin decomposition is presumed to be responsible for the exothermic thermal behavior in the final stage of wood pyrolysis. The effect of exothermic lignin decomposition was studied by using model-2 which consists of hemicellulose, cellulose and lignin pyrolysis models. The kinetics parameters of each model were taken from the literature as described in the previous section. The heat of pyrolysis,  $\Delta h$  of hemicellulose, cellulose and lignin decompositions were found by fitting to the experimental result as:  $\Delta h_{hcl} = 100$  kJ/kg,  $\Delta h_{cl} = 280$  kJ/kg and  $\Delta h_l = -350$  kJ/kg. This was done to determine if the model can reproduce the observed trends despite the constants. Fig. 6 shows solid mass fraction comparison between the experiment and model-2 for different temperature conditions. Since pre-determined fixed char yield ratios are used for pyrolysis models of all three components, the final char of model-2 does not account for the final char yield variation for different temperature conditions observed in the experiments. As a result, except for the 688 K case, the final char yield of model-2 is different from

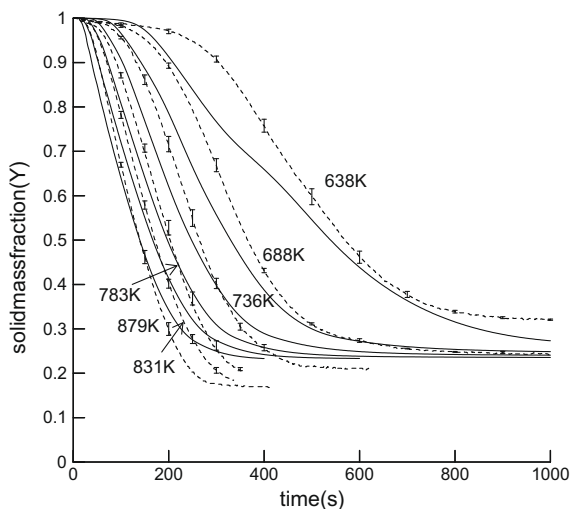


Fig. 6. Solid mass fraction comparison between model-2 and experiment (solid line: model-2, dotted line: experiment).

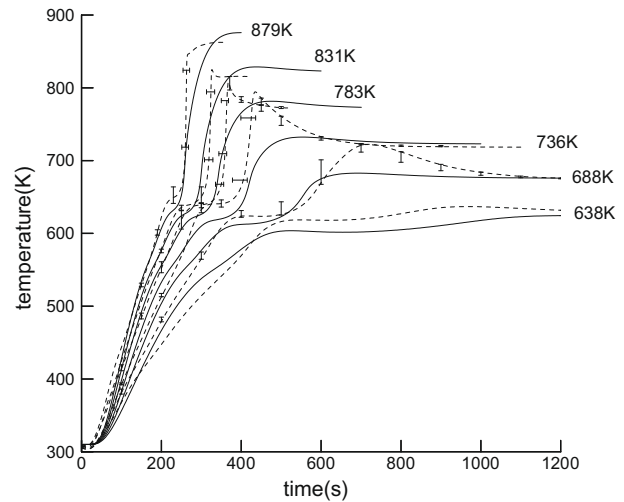


Fig. 7. Center temperature comparison between model-2 and experiment (solid line: model-2, dotted line: experiment).

the experiments. Also, model-2 predicts faster solid mass loss rate in the beginning stage due to the hemicellulose pyrolysis and slow lignin decomposition results in a gradual slope in the final stage. In general, the mass loss predictions of model-2 are not satisfactory as shown in Fig. 6. The discrepancy is believed to be for the following reasons: (i) Pure cellulose, hemicellulose and lignin used to determine the decomposition kinetics do not have the same chemical structure as those existing in wood. (ii) The interaction among components would affect the individual pyrolysis of each component, which is not considered in model-2. However owing to separate modeling of hemicellulose, cellulose and lignin, model-2 reproduces the characteristics of experimental solid mass loss in the beginning and the final stage better than model-1 (not shown).

Fig. 7 shows the center temperature (at  $r = 0$ ) comparison between model-2 and the experiments. The center temperature plateau predicted by model-2 agrees well with the experiments in both magnitude and duration. Individual modeling of each component, especially cellulose decomposition which is strongly endothermic, enables good prediction of the center temperature plateau. On the other hand, the temperature rise after the plateau is gradual and the magnitude of the exothermic center temperature peak is small compared with the experiments. This is despite using the best-fit values for the heats of pyrolysis.

Decomposition rates of the three components at the center of the sphere are plotted in Fig. 8. Hemicellulose and cellulose decomposition appear as two distinct peaks in sequential order. The cellulose decomposition peak corresponds to the center temperature plateau in Fig. 7. The results indicate that the first and second parts of the main mass loss period correspond to hemicellulose and cellulose decomposition respectively. In the experiment, the center temperature plateau corresponds to the second part of the mass loss period. Therefore, the center temperature plateau is caused by endothermic cellulose decomposition. Hemicellulose decomposition is less endothermic than cellulose.

Lignin decomposition occurs over a wide temperature range. It begins earlier and lasts longer than the other two components. Since the lignin decomposition rate is less sensitive to temperature than other components, more lignin is left after the completion of endothermic cellulose decomposition for the 831 K case than the 688 K case. As a result, the exothermic effect is more evident for the 831 K case than the 688 K case in the calculations. This is not consistent with the experiments that show a more distinct center temperature peak for the 688 K. Further, the center temperature rise after the temperature plateau is gradual, owing to gradual

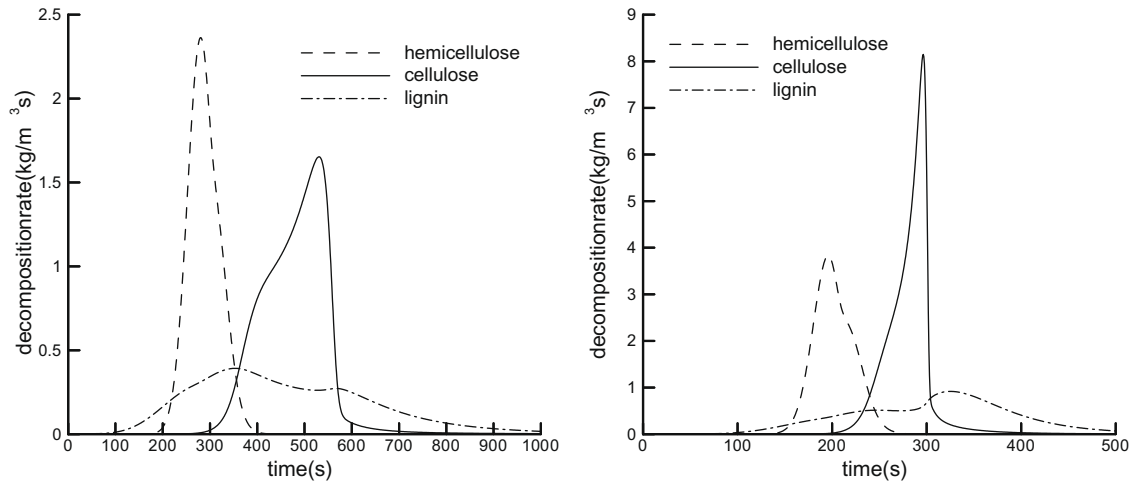


Fig. 8. Decomposition rate of three components at the center of the wood sphere; furnace temperature (a) 688 K, (b) 831 K, model-2.

Table 8  
Furnace and gas temperatures.

$T_{fn}$	638	688	736	783	831	879
$T_g$	585	635	670	720	770	820

Table 9  
Model-3 kinetic parameters and  $\Delta h$ .

Reaction	1	2	3
$A_i$ ( $s^{-1}$ )	$2.00 \times 10^{10}$	$2.51 \times 10^7$	$1.38 \times 10^{10}$
$E_i$ (J/mol)	148,000	117,000	161,000
$\Delta h$ (kJ/kg)	110	0	-210

exothermic lignin decomposition. Since the center temperature rise for model-2 is different from the experiments, it is concluded that the exothermic behavior observed in the experiment is not primarily caused by exothermic lignin decomposition.

4.2.3. Intermediate solid decomposition

For cellulose pyrolysis, several researchers [8,9] have reported an exothermic reaction following the endothermic reaction, with the exothermic reaction being attributed to the exothermic decomposition of dehydrocellulose to char and gas. Since cellulose comprises approximately half of the wood mass, it is plausible to assume wood pyrolysis process as similar to cellulose pyrolysis. The effect of the exothermic intermediate solid (corresponding to dehydrocellulose in cellulose pyrolysis) decomposition to char and gas was studied using model-3 to determine its role in the exothermic behavior of the wood pyrolysis. Kinetic parameters used in model-3 are listed in Table 9. Activation energy  $E_1$  is taken from the tar producing reaction of model-1. Other kinetic parameters and  $\Delta h$  are found by fitting with the experimental results.

As shown in Fig. 9, solid mass fractions predicted by model-3 shows good agreement with the experiments, except for the 638 K case. The center temperature peak of model-3 also agrees well with the experiment, as shown in Fig. 10. In addition, model-3 shows a decrease of the temperature peak at higher furnace temperature, as observed in the experiments.

The exothermic secondary decomposition of the intermediate solid seems plausible for the following reasons. (i) The center temperature peak appears after the active mass loss process and only small or negligible mass loss occurs during the exothermic reaction period. This indicates that the reactants of the exothermic reaction

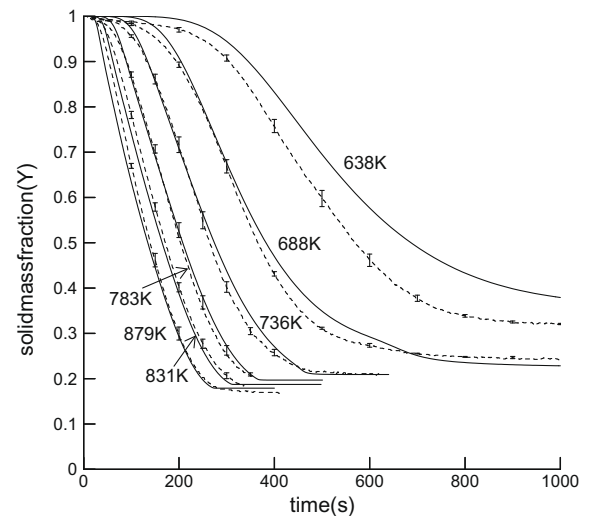


Fig. 9. Solid mass fraction comparison between model-3 and experiment (solid line: model, dotted line: experiment).

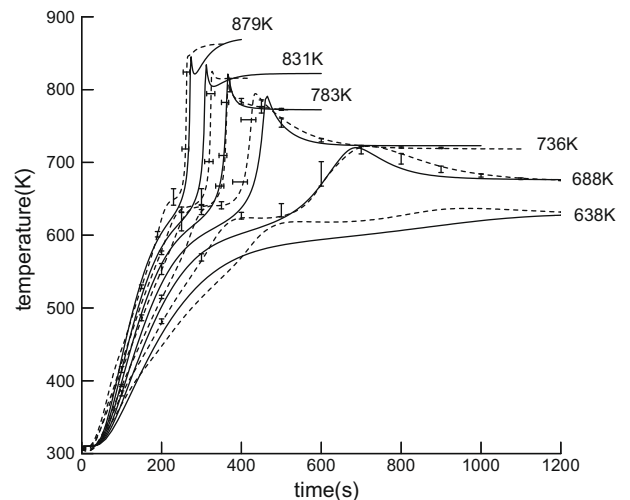


Fig. 10. Center temperature comparison between model-3 and experiment (solid line: model, dotted line: experiment).

**Table 10**  
Proposed model kinetic parameters and  $\Delta h$ .

Reaction	t	g	is	c	c2	g2
$A_i$ ( $s^{-1}$ )	$1.08 \times 10^{10}$	$4.38 \times 10^9$	$3.75 \times 10^6$	$1.38 \times 10^{10}$	$1.0 \times 10^5$	$4.28 \times 10^6$
$E_i$ (J/mol)	148,000	152,700	111,700	161,000	108,000	108,000
$\Delta h_i$ (kJ/kg)	80	80	80	-300	-42	-42

are in the solid phase and the product are also primarily in the solid phase, i.e. char. (ii) Exothermicity increases with the increase of char yield. (iii) The endothermic reaction and the exothermic reaction occur in consecutive order. (iv) It is possible that thermodynamically the solid rearranges to a more stable form (char) releasing energy.

From the relationship between char yield and the furnace temperature, it is evident that the char producing process prefers lower temperature, whereas volatiles generation is promoted at higher temperature. Thus, the intermediate solid reaction begins earlier (has a lower activation energy) than the volatiles generation process. However, the exothermic reaction related to char conversion occurs in the final stage of pyrolysis. Therefore, the exothermic reaction cannot be the primary char forming reaction which is competing with the volatiles producing reaction from virgin wood. Hence, it is concluded that the char forming process satisfying the experimental observations should be a two-step reaction process, whereby an intermediate solid is introduced. The first reaction is virgin solid to intermediate solid conversion which is competing with volatiles forming reaction and prefers lower temperature. This non-exothermic reaction determines the char yield. The second reaction is the exothermic conversion of the intermediate solid to char or both char and gas as in model-3.

Despite this encouraging thermal behavior, the center temperature plateau of model-3 is not as distinct as that predicted by model-2, because wood is modeled as a single material as in model-1. However, satisfactory model prediction for both the thermal behavior and the mass loss were achieved by model-3.

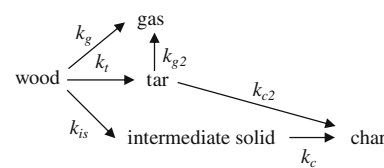
To summarize, the results of model-3 showed reasonable agreement with the experiments where the exothermic behavior appears after the endothermic wood pyrolysis reaction. This exothermicity is attributed to the exothermic intermediate solid decomposition to char and gas.

## 5. Modeling of endo/exothermic wood pyrolysis

A new wood pyrolysis model is proposed based on the experimental and theoretical results of this work. This model accounts for the observed endo/exothermic thermal behavior and the solid mass loss measured in the experiments. In addition, the model predicts product yield satisfactorily for the application to liquid bio-fuel production.

There is considerable experimental evidence [11,18] that suggests that there is competition between gas, char, and tar yield during wood pyrolysis which depends on the heating conditions. For long intraparticle volatile residence time, gas yield increases at high pyrolysis temperatures, whereas, char yield increases at low temperature. In model-3, since both char and gas are produced from the intermediate solid at a fixed ratio between them, the resulting gas yield is not realistic. Thus, the gas producing reaction must be one of the primary competing reactions rather than the secondary decomposition of the intermediate solid. Further, it is well-known that to increase the tar (condensable volatiles-liquid) yield short volatile residence times are needed. Hence, the reaction mechanism should also include a secondary tar cracking step. Thus, the proposed model is a modified form of model-1 which employs a two-step char producing reaction similar to model-3.

However, unlike model-3, intermediate solid is converted only to char and gas is produced directly from the virgin wood by a primary reaction. Kinetics parameters of primary and secondary tar decomposition reactions are taken from model-1, except for  $A_{is}$  which is adjusted by experimental mass loss data from this work. Kinetic parameters of reaction c come from reaction 3 of model-3. Kinetic parameters of the proposed model are listed in Table 10 and a summary of equations describing this model are given below.



### 5.1. Mass conservation

Mass conservation of each component is governed by diffusive and convective mass flux in the gas phase and production or destruction owing to the decomposition reactions. It is assumed that volume shrinkage does not occur. Material properties and reaction parameters used in equations are listed in Table 7.

The mass change per unit volume of each solid phase component depends on the pyrolysis reactions.

$$\text{Virgin wood : } \frac{\partial \rho_a}{\partial t} = S_a = -(k_t + k_g + k_{is})\rho_a \quad (2)$$

$$\text{Intermediate solid : } \frac{\partial \rho_{is}}{\partial t} = S_{is} = k_{is}\rho_a - k_c\rho_{is} \quad (3)$$

$$\text{Char : } \frac{\partial \rho_c}{\partial t} = S_c = k_c\rho_{is} + k_{c2}\rho_t \quad (4)$$

Mass change per unit volume of each gas phase component can be expressed as the sum of mass flux through the control volume boundaries and mass generation in the volume due to the pyrolysis reaction. The mass flux of each gaseous species consists of convective flux due to gas flow and diffusive flux due to diffusion among the gaseous species. However, since the effect of the diffusion is very small compared to the convection, only the convective mass flux is considered here. Equations are written in spherical coordinates.

$$\text{Tar : } \frac{\partial(\varepsilon\rho_t)}{\partial t} + \frac{1}{r^2} \frac{\partial}{\partial r}(r^2V\rho_t) = S_t = k_t\rho_a - (k_{c2} + k_{g2})\rho_t \quad (5)$$

$$\text{Gas : } \frac{\partial(\varepsilon\rho_g)}{\partial t} + \frac{1}{r^2} \frac{\partial}{\partial r}(r^2V\rho_g) = S_g = k_g\rho_a + k_{g2}\rho_t \quad (6)$$

where  $\varepsilon$  is the porosity calculated by  $\varepsilon = 1 - \frac{\rho_s}{\rho_w}(1 - \varepsilon_w)$ . Here,  $\rho_s$  and  $\rho_w$  are the total solid and virgin wood masses per unit volume,  $\varepsilon_w$  is initial wood porosity,  $\varepsilon_w = 0.4$  [25].

Since the wood and char structure is composed of numerous tiny pores, the internal gaseous components flow is dominated by the viscous force. Thus, the gaseous components flow velocity  $V$  is calculated by Darcy's law.

$$V = -\frac{B}{\mu} \frac{\partial P}{\partial r} \quad (7)$$

where  $\mu$  is the viscosity.

The permeability  $B$  of partially pyrolyzed solid is linearly interpolated between char and virgin wood as

$$B = (1 - \eta)B_w + \eta B_c \quad (8)$$

where the degree of pyrolysis is  $\eta = 1 - \frac{\rho_a + \rho_g}{\rho_w}$ .

Pressure is the sum of the partial pressures of tar and gas that are assumed to behave as ideal gases at these temperatures.

$$P = P_t + P_g; \quad P = \frac{\rho RT}{M} \quad (9)$$

where  $M$  and  $R$  are molecular weight and the universal gas constant.

Combining Eqs. (5)–(9) gives the total pressure equation.

$$\begin{aligned} \text{Total Pressure : } & \frac{\partial}{\partial t} \left( \frac{\varepsilon P}{T} \right) - \frac{1}{r^2} \frac{\partial}{\partial r} \left( r^2 \frac{BP}{\mu T} \frac{\partial P}{\partial r} \right) \\ & = \left( \frac{R}{M_t} S_t + \frac{R}{M_g} S_g \right) \end{aligned} \quad (10)$$

Eq. (10) is nonlinear and numerically difficult to solve. The accuracy of the numerical solution was tested against the exact analytical solution given in Ref. [14].

### 5.2. Energy conservation

The conservation of energy is governed by the change of energy stored in the control volume by thermal conduction, convective flow of gas phase components, and heat generation by the pyrolysis reaction. In order to setup the energy equation, local thermodynamic equilibrium between gas and the solid phase components is assumed.

$$\begin{aligned} (C_w \rho_a + C_w \rho_{is} + C_c \rho_c + \varepsilon C_{pt} \rho_t + \varepsilon C_{pg} \rho_g) \frac{\partial T}{\partial t} + (C_{pt} \rho_t \\ + C_{pg} \rho_g) V \frac{\partial T}{\partial r} = \frac{1}{r^2} \frac{\partial T}{\partial r} \left( r^2 \lambda \frac{\partial T}{\partial r} \right) + Q \end{aligned} \quad (11)$$

where,  $Q = -(k_t \Delta h_t + k_g \Delta h_g + k_{is} \Delta h_{is}) \rho_a - k_c \Delta h_c \rho_{is} - (k_{c2} \Delta h_{c2} + k_{g2} \Delta h_{g2}) \rho_t$

The primary reactions  $t$ ,  $g$  and  $is$  have the same endothermic heat of pyrolysis,  $\Delta h_t = \Delta h_g = \Delta h_{is} = 80$  kJ/kg and the second step exothermic reaction  $c$  has  $\Delta h_c$  of  $-300$  kJ/kg. These values were determined by matching with the experiments. The kinetic parameters and  $\Delta h$  of tar cracking reactions are the same as those used in model-1.

Specific heat capacity for solid components  $C$  and constant pressure specific heat capacity  $C_p$  for the gaseous components are functions of temperature as shown in Table 7. Effective thermal conductivity  $\lambda$  at any instant is calculated as the weighted sum

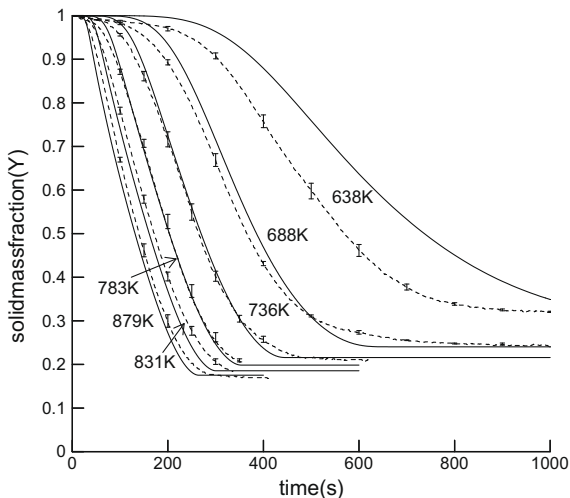


Fig. 11. Solid mass fraction comparisons between the proposed model and experiments (solid line: proposed model, dotted line: experiment).

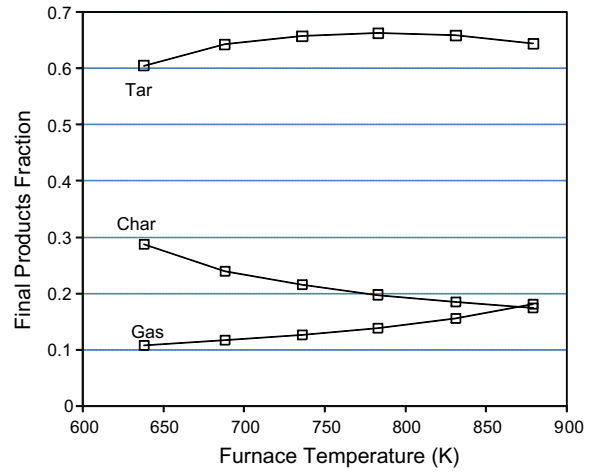


Fig. 12. Final product fractions for the proposed model.

of virgin wood, char and volatiles conductivity and accounting for radiation heat transfer through the pore [26].

$$\lambda = (1 - \eta) \lambda_w + \eta \lambda_c + \varepsilon \lambda_v + \frac{13.5 \sigma T^3 d}{e} \quad (12)$$

where  $\sigma$ ,  $e$  and  $d$  are the Stefan–Boltzmann constant, emissivity and pore size.

It is well-known that the thermal conductivity of unpyrolyzed wood along the grain is about 2.4 times the thermal conductivity in the radial or tangential direction [26]. Thermal conductivity also varies significantly with location within the sample and between different samples. This anisotropic and inhomogeneous behavior is approximated to enable a 1-D model. Thus, the thermal conductivity used for the 1-D model is taken as the average value of the three directions (radial, tangential and grain) for both wood and char with radial and tangential being equal.

$$\begin{aligned} \lambda_w &= (\lambda_{w,\text{radial}} + \lambda_{w,\text{tangential}} + \lambda_{w,\text{grain}}) / 3 \quad \text{and} \\ \lambda_c &= (\lambda_{c,\text{radial}} + \lambda_{c,\text{tangential}} + \lambda_{c,\text{grain}}) / 3 \end{aligned} \quad (13)$$

While this is approximate, the error is expected to be small and it saves considerable amount of computational time. Ozisik [35] shows that for constant ' $\lambda_{w,i}$ ', by appropriately scaling the coordi-

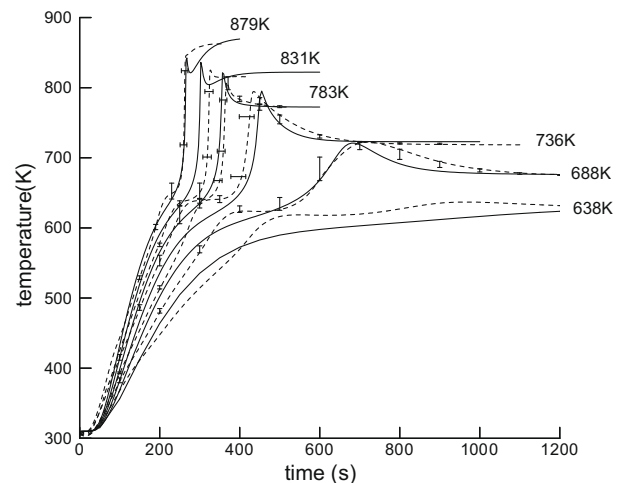


Fig. 13. Center temperature comparisons between the proposed model and the experiment (solid line: proposed model, dotted line: experiment).

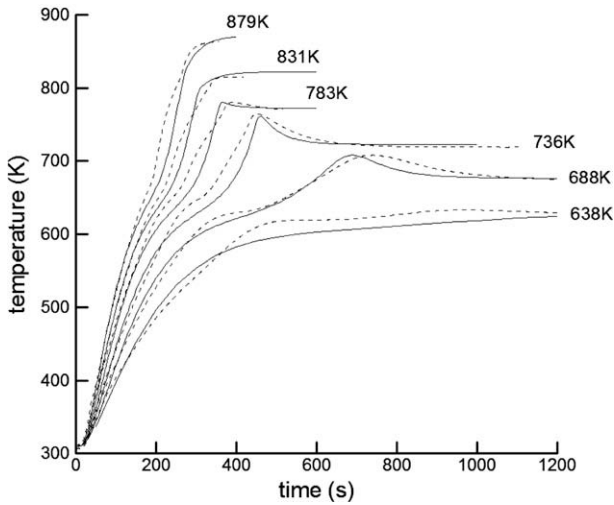


Fig. 14. Middle temperature comparisons between the proposed model and the experiment (solid line: proposed model, dotted line: experiment).

nates by  $\sqrt{\lambda_w/\lambda_{w,i}}$  the anisotropic conduction equation may be converted into an isotropic equation. Using Ozisik's method yields  $\lambda_{w,ave} = 1.36 \times \lambda_{w,radial}$ , where  $\lambda_{w,radial} = \lambda_{w,tangential}$ , whereas using the average thermal conductivity yields  $\lambda_{w,ave} = 1.47 \times \lambda_{w,radial}$ , an error of 8% which is well within the natural variation. This is considered acceptable because shrinkage is not considered and thermal conductivity changes with temperature, extent of decomposition and shrinkage. The benefit of using the average value is that it eliminates the need for transforming the solution back to the original physical coordinates.

Thermal energy flux through the wood sphere boundary surface is determined by external convective and radiative heat transfer conditions by:

$$\frac{\partial T}{\partial r} = h(T_g - T) + \sigma e_s(T_f^4 - T^4); \quad (r = r_0) \quad (14)$$

Furnace and argon temperatures surrounding the sample 'T<sub>g</sub>' are listed in Table 8.

Surface emissivity is calculated according to [25]:

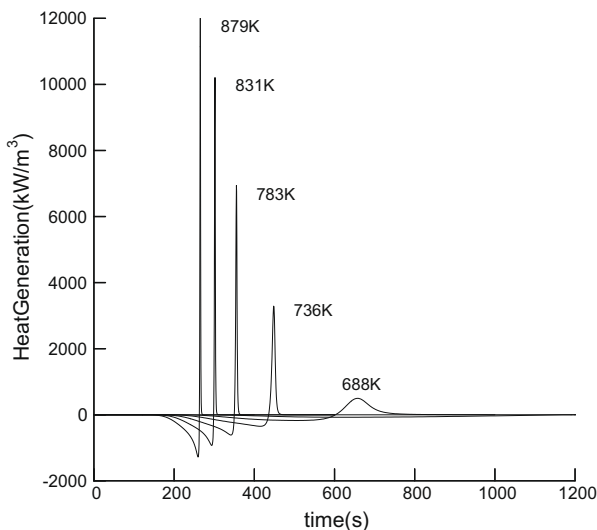


Fig. 15. Heat generation rate at the sample center.

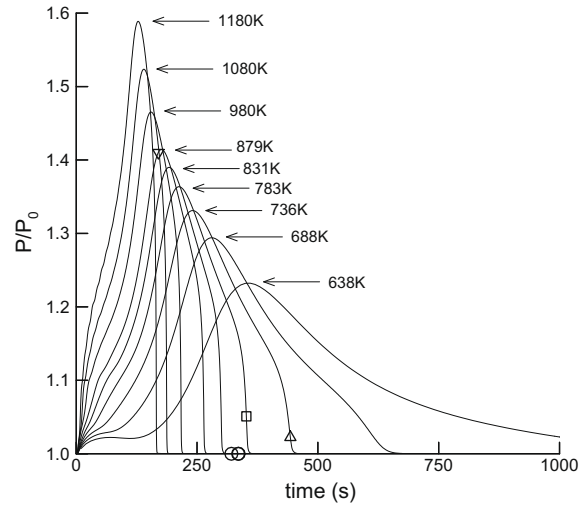


Fig. 16. Center pressure for the proposed model (solid lines: pressure  $P/P_0$ , symbols: sample split during the experiments).

$$\begin{cases} e_s = e_w & T_s < 450 \text{ K} \\ e_s = e_w + \frac{T_s - 450}{550 - 450} (e_c - e_w) & 450 \text{ K} \leq T_s \leq 550 \text{ K} \\ e_s = e_c & 550 \text{ K} < T_s \end{cases} \quad (15)$$

The surface convective heat transfer coefficient is estimated to be  $h = 20 \text{ W/m}^2 \text{ K}$ . It is difficult to find an accurate value of 'h' near the sphere surface because the flow around it is quite complicated. Preliminary CFD calculations (using fluent) inside the furnace showed that there is recirculating flow caused by buoyancy. The gas temperature near the wall is hotter than the gas at the center-line. Thus, we estimated 'h' by matching the final temperatures of the sphere surface (Fig. 3). At the final stage, there is no temperature gradient inside the sphere ( $T_{\text{surface}} = T_{\text{center}}$ ) and the surface temperature is governed by the energy balance between radiation and convection heat transfer. The sphere temperature is between the gas temperature and the furnace temperature. This was confirmed by gas temperature measurements near the sample surface. Thus, convection cooling equals radiative heating yielding an average value of the convective heat transfer coefficient 'h'. Measure-

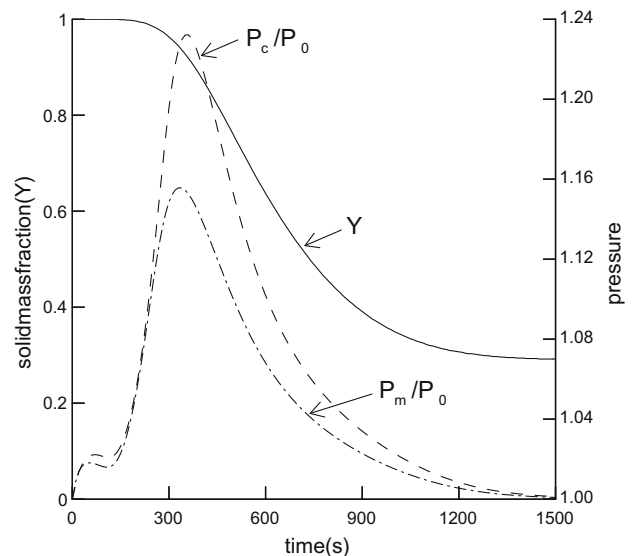
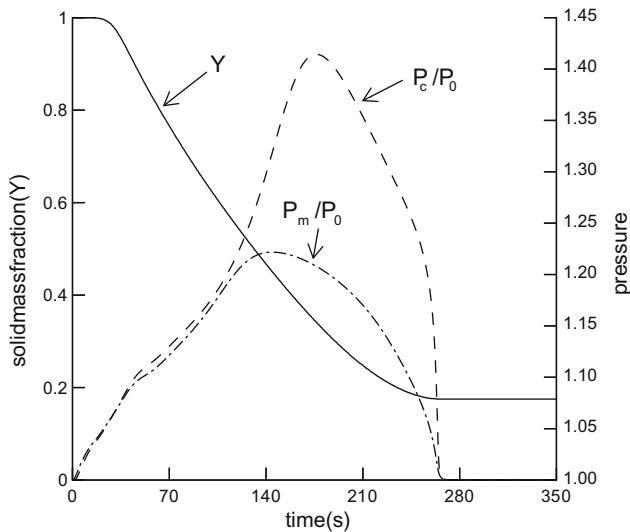


Fig. 17. Pressures at center and middle locations and solid mass fraction (Y) for furnace temperature 638 K.



**Fig. 18.** Pressures at center and middle locations and solid mass fraction ( $Y$ ) for furnace temperature 879 K.

ments of gas temperature near the sample surface showed that it was uniform around the sphere to within 10 °C, with no particular distinction between top and bottom due to recirculating flow inside the furnace. Given the fact that the sphere changed shape during pyrolysis and that there was blowing of the pyrolysis gases from the sphere, this symmetry was considered acceptable and an average value of ‘ $h$ ’ was used.

## 6. Model results

Computed solid mass fractions for the proposed model are compared with the experiments in Fig. 11. In general, a good agreement is seen except for the 638 K case. While 736 K and higher temperature cases show better agreement with the experiments, the solid mass loss characteristics at the beginning and in the final stages of pyrolysis are not predicted as well by the proposed model. Solid mass of the proposed model remains constant until the initial mass loss begins, whereas some solid mass loss was observed from the beginning in the experiments. In the final stage of wood pyrolysis, the proposed model shows a distinct end of solid mass loss, whereas a gradual solid mass loss was observed in the experiments. This discrepancy may be attributed to the limitations of the 1st order Arrhenius kinetics that focuses on the primary pyrolysis process [27]. Consequently, the kinetics scheme better represents the cellulose decomposition which is the primary part of the wood pyrolysis. On the other hand, low temperature hemicellulose decomposition in the beginning stage and high temperature lignin decomposition in the final stage are not taken into account as well in proposed model. Large solid mass discrepancy between the model and the 638 K experiment is attributed to the incapability of the proposed mechanism to model low temperature pyrolysis, which may be acceptable for bio-oil production, which requires higher temperatures. Final product fractions of the proposed model are plotted in Fig. 12. As temperature increases, more volatiles and less char are produced. For furnace temperatures higher than 750 K, secondary tar decomposition influences tar and gas yields. Tar (condensable hydrocarbons) yield for the model decreases for temperature higher than 800 K due to secondary tar decomposition.

Figs. 13 and 14 show that the model predictions of the center and the middle temperatures compare well with the experiments. The temperature peaks are well predicted by the two-step char producing reactions. However, the temperature plateaus of the

proposed model are not as distinct as seen in the experiments. The approximation of a single wood reactant leads to gradual temperature change during endothermic pyrolysis rather than distinct plateau observed during the experiments and predicted by model-2. The exothermic peaks in Figs. 13 and 14 correspond to the center and middle temperature rise. While the center temperature for the high temperature cases did not rise above the surface temperature (Fig. 3), heat generation rate was significant. This heat generation at the center of the wood sphere during pyrolysis is shown in Fig. 15. The generated heat quickly heats up the sample interior and contributes to significant pressure generation inside the sample.

## 7. Pressure generation

Pressure variations at the center of the wood sphere for the furnace temperature range  $T_{fn} = 638\text{ K} - 1180\text{ K}$  are shown in Fig. 16. The magnitude of the pressure peak increases with the furnace temperature becoming almost 1.6 atmospheres at 1180 K. The pressure profiles have different shapes for different furnace temperatures. At all furnace temperatures and early times, the particle quickly develops a small internal pressure to push the gases out that are mostly expanded air because the solid has lost very little mass at this time. Subsequently, at high furnace temperatures, the center pressure rises steadily until the pressure peak and then it drops rapidly to the ambient pressure. At low furnace temperatures, the center pressure rises to the peak pressure relatively quickly but drops to the ambient pressure gradually. This observation indicates that pressure peak occurs at different stages of pyrolysis depending on the furnace temperature. Center ( $r = 0$ ) and middle ( $r = r_o/2$ ) pressures are shown along with the solid mass fraction for  $T_{fn} = 638\text{ K}$  and  $T_{fn} = 879\text{ K}$  in Figs. 17 and 18 respectively. At  $T_{fn} = 638\text{ K}$ , pressure peak appeared at  $\eta = 11.4$ . In contrast, at  $T_{fn} = 879\text{ K}$ , pressure peak occurred at  $\eta = 79.9$ . Although the center pressure is always higher than the middle pressure, the reason for the pressure peaks occurring at different extents of pyrolysis may be explained as follows: At lower temperatures, the sample is heated slowly and the temperature gradient along the radial direction is small. This results in a wide pyrolysis zone in the radial direction. Since the virgin solid permeability is significantly smaller than that of the char and the permeability is slowly increasing everywhere due to partial pyrolysis, a permeability gradient exists in the pyrolysis zone. Thus, while the volatiles generation rate is small, the permeability is also small resulting in a pressure peak at lower extent of pyrolysis. Thus, the pressure peak is caused by small permeability and not by large volatile generation. At higher temperatures, the pyrolysis zone is relatively thin and the surface has much higher permeability than the center. Thus the resistance offered by the partially pyrolyzed solid is small. Pressure build up is thus the result of large volatiles flow in thick char and thin partially pyrolyzed wood. As a result, the pressure peak appears near the end of pyrolysis when volatiles have to travel the longest path through the char. In the experiments, sample split was observed for some cases especially at higher temperatures. Fig. 16 shows these events along with the center pressure and Fig. 1b shows a photograph of a split sample. The event of sample split was identified by either a sudden mass loss of the sample or a sudden change of temperature measurement when the center thermocouple was exposed to furnace atmosphere. This split is caused by internal pressure, cracks due to non-uniform shrinkage, and structural weakness due to charring.

It is useful to examine the relation between internal pressure and sample split shown in Fig. 16. The split did not occur for low temperature cases  $T_{fn} = 638\text{ K}$  and  $688\text{ K}$ . At low temperature, the pressure peak is small and appears in early stage of pyrolysis when the sample structure has not been weakened. In the mid

temperature region, the sample split occurs at the end of the pyrolysis when most of the sample was converted to char. Thus in the mid temperature region, the sample split is dominated by structural weakness rather than internal pressure. At high temperatures  $T_{fm} = 879$  K, the sample split event was coincident with the pressure peak when its structure has weakened and could not endure the internal pressure. Sample split is not shown for temperatures higher than  $T_{fm} = 879$  K because experiments were not performed for those temperatures. However, it is expected that the sample would be split at the pressure peak or before reaching the pressure peak. In that case, the actual internal pressure may not reach the predicted pressure peak.

## 8. Conclusions

Pyrolysis of moisture-free wood spheres has been studied both experimentally and theoretically. Temperature measurements show two distinct sequential thermal regimes during wood pyrolysis. First, an endothermic reaction that causes a center temperature plateau. During this period, a large amount of solid mass loss occurs. Second, a steep temperature rise with the center temperature peak exceeding the surface temperature. This occurs after the center temperature plateau. A small or negligible amount of solid mass loss occurs during this exothermic reaction period. Therefore, the endothermic period corresponds to primary reactions of active volatiles generation, especially cellulose decomposition, and the exothermic period corresponds to the conversion of the intermediate solid to final char. This is confirmed by a numerical study of various endothermic and exothermic mechanisms in conjunction with the experimental measurements. Thus the exothermic intermediate solid decomposition is responsible for the center temperature peak. The contributions of the secondary tar decomposition and lignin decomposition to the center temperature peak are small. Further, the results of the mixture model (model-2) indicate that endothermic cellulose decomposition is responsible for the center temperature plateau.

A new wood pyrolysis model is proposed based on this experimental and theoretical study. The model consists of three endothermic parallel reactions for tar, gas and intermediate solid and a subsequent exothermic conversion of the intermediate solid to char and the secondary tar decomposition mechanism. Comparison between the model and experiments show good agreement with both the temperature and the solid mass loss measurements. Further, this model is consistent with other observations of product yield in the literature.

Pressure calculations with the new pyrolysis model revealed that the internal pressure build up mechanism is different at different furnace temperatures. At high temperatures, a thick wood particle may split by combination of high internal pressure and weakened structure. On the other hand, a thick wood particle does not split during low temperature pyrolysis. Therefore, pressure becomes more important for the high temperature fast pyrolysis process.

## Acknowledgments

The research at the University of Michigan was supported by NIST Grant # 3D1086.

## References

- [1] G.W. Huber, (Ed.), National Science Foundation Report. Breaking the Chemical and Engineering Barriers to Lignocellulosic Biofuels: Next Generation Hydrocarbon Biorefineries, Chemical, Bioengineering, Environmental, and Transport Systems Division. Washington, DC, 2008, 180 p.
- [2] R.D. Perlack, L.L. Wright, A.F. Turhollow, R.L. Graham, B.J. Stokes, D.C. Erbach, Biomass as feedstock for a bioenergy and bioproducts industry: the technical

- feasibility of a billion-ton annual supply. A joint study sponsored by US Department of Energy and US Department of Agriculture, April, 2005.
- [3] J. Fargione, J. Hill, D. Tilman, S. Polasky, P. Hawthorne, Land Clearing and the Biofuel Carbon Debt, Published online February 7, 2008, doi: 10.1126/science.1152747.
- [4] T.R. Carlson, T.P. Vispute, G.W. Huber, Green gasoline by catalytic fast pyrolysis of solid biomass derived compounds, *ChemSusChem* 1 (2008) 397–400.
- [5] R. Bilbao et al., Modelling of the pyrolysis of wet wood, *Journal of Analytical and Applied Pyrolysis* 36 (1) (1996) 81–97.
- [6] C. Di Blasi et al., Pyrolytic behavior and products of some wood varieties, *Combustion and Flame* 124 (1–2) (2001) 165–177.
- [7] C.A. Koufopoulos et al., Modelling of the pyrolysis of biomass particles. Studies on kinetics, thermal and heat transfer effects, *Canadian Journal of Chemical Engineering* 69 (4) (1991) 907–915.
- [8] I. Milosavljevic, V. Oja, E.M. Suuberg, Thermal effects in cellulose pyrolysis: relationship to char formation processes, *Industrial and Engineering Chemistry Research* 35 (3) (1996) 653.
- [9] V. Strezov, B. Moghtaderi, J. Lucas, Thermal study of decomposition of selected biomass samples, *Journal of Thermal Analysis and Calorimetry* 72 (3) (2003) 1041–1048.
- [10] A. Atreya, *Pyrolysis, Ignition and Flame Spread on Horizontal Surfaces of Wood*, Ph.D. thesis, Harvard University, Cambridge, MA, 1983.
- [11] M.G. Gronli, M.C. Melaaen, Mathematical model for wood pyrolysis – comparison of experimental measurements with model predictions, *Energy & Fuels* 14 (4) (2000) 791–800.
- [12] I. Milosavljevic, E.M. Suuberg, Cellulose thermal decomposition kinetics: global mass loss kinetics, *Industrial and Engineering Chemistry Research* 34 (4) (1995) 1081–1091.
- [13] B. Fredlund, A Model for Heat and Mass Transfer in Timber Structures During Fire, A Theoretical, Numerical and Experimental Study in Report LUTVDG/TVBB-1003. Lund University, Sweden, 1988.
- [14] H.R. Baum, A. Atreya, A model of transport of fuel gases in a charring solid and its application to opposed-flow flame spread, *Proceedings of the Combustion Institute* 31 (2) (2007) 2633–2641.
- [15] W.C. Park, A. Atreya, H.R. Baum, Numerical study of thermal decomposition and pressure generation in charring solids undergoing opposed-flow flame spread, *Proceedings of the Combustion Institute* 31 (2) (2007) 2643–2652.
- [16] R. Siegel, J.R. Howell, *Thermal Radiation Heat Transfer*, fourth ed., Taylors & Francis, New York, USA, 2002.
- [17] C. Di Blasi, Modeling intra- and extra-particle processes of wood fast pyrolysis, *AIChE Journal* 48 (10) (2002) 2386–2397.
- [18] D. Mohan, C.U. Pittman Jr., P.H. Steele, Pyrolysis of wood/biomass for bio-oil: a critical review, *Energy & Fuels* 20 (3) (2006) 848–889.
- [19] G. Varhegyi et al., Kinetics of the thermal decomposition of cellulose, hemicellulose, and sugar cane bagasse, *Energy & Fuels* 3 (3) (1989) 329–335.
- [20] R. Capart, L. Khezami, A.K. Burnham, Assessment of various kinetic models for the pyrolysis of a microgranular cellulose, *Thermochimica Acta* 417 (1) (2004) 79–89.
- [21] R.W.C. Chan, B.B. Krieger, Kinetics of dielectric-loss microwave degradation of polymers: lignin, *Journal of Applied Polymer Science* 26 (5) (1981) 1533–1553.
- [22] E. Sjostrom, *Wood Chemistry Fundamentals and Applications*, Academic Press, New York, NY, 1981.
- [23] F.J. Kilzer, A. Broido, Speculation on the nature of cellulose pyrolysis, *Pyrodynamics* 2 (1965) 151.
- [24] W.S.L. Mok, M.J. Antal, Effects of pressure on biomass pyrolysis. II. Heats of reaction of cellulose pyrolysis, *Thermochimica Acta* 68 (2–3) (1983) 165–186.
- [25] A. Galgano, C.D. Blasi, Modeling wood degradation by the unreacted-core-shrinking approximation, *Industrial & Engineering Chemistry Research* 42 (10) (2003) 2101–2111.
- [26] C. Di Blasi, Heat momentum, Heat, momentum, and mass transport through a shrinking biomass particle exposed to thermal radiation, *Chemical Engineering Science* 51 (7) (1996) 1121–1132.
- [27] C. Di Blasi, C. Branca, Kinetics of primary product formation from wood pyrolysis, *Industrial & Engineering Chemistry Research* 40 (23) (2001) 5547–5556.
- [28] C. Di Blasi, Analysis of convection and secondary reaction effects within porous solid fuels undergoing pyrolysis, *Combustion Science and Technology* 30 (1993) 315–340.
- [29] A.G. Liden, F. Berruti, D.S. Scott, A kinetic model for the production of liquids from the flash pyrolysis of biomass, *Chemical Engineering Communications* 65 (1988) 207–221.
- [30] W.C. Park, A Study of Pyrolysis of Charring Materials and Its Application to Fire Safety and Biomass Utilization in Mechanical Engineering, The University of Michigan, Ann Arbor, 2008.
- [31] W.-C.R. Chan, M. Kelbon, B.B. Krieger, Modelling and experimental verification of physical and chemical processes during pyrolysis of a large biomass particle, *Fuel* 64 (11) (1985) 1505–1513.
- [32] C.K. Lee, R.F. Chaiken, J.M. Singer, Charring pyrolysis of wood in fires by laser simulation, *Proceedings of the Combustion Institute* (1976) 1459–1470.
- [33] C. Di Blasi, Modelling the fast pyrolysis of cellulosic particles in fluid-bed reactors, *Chemical Engineering Science* 55 (24) (2000) 5999–6013.
- [34] E.J. Kansa, H.E. Perlee, R.F. Chaiken, Mathematical model of wood pyrolysis including internal forced convection, *Combustion and Flame* 29 (1977) 311–324.
- [35] N.M. Ozisik, *Heat Conduction*, first ed., John Wiley and Sons, New York, NY, USA, 1980.